Draft version February 25, 2014
Preprint typeset using LaTeX style emulateapj v. 12/16/11

PRIMUS: QUIESCENT FRACTION AS A FUNCTION OF ENVIRONMENT AND REDSHIFT

ChangHoon Hahn, Michael Blanton, Alison Coil, Richard Cool, Daniel Eisenstein, John Moustakas, Ken Wong, Guangtun Zhu

Draft version February 25, 2014

ABSTRACT

We examine the evolution of the quiescent fraction (QF) for galaxies in different density environments from $z = 0.2 - 0.8$ using spectroscopic redshift and multi-wavelength imaging data from PRism MUlti-object Survey (PRIMUS) and the Sloan Digitial Sky Survey (SDSS). Using this data we construct a stellar mass limited target galaxy population of 40430 galaxies from PRIMUS within redshift range $0.2 - 1.0$ and 106732 galaxies from SDSS within redshift range $0.06 - 0.145$. This population is then classified as quiescent or star-forming using an evolving cut based on specific star-formation rate. The environment of the target population is then measured using a fixed cylindrical aperture method on a volume-limited *Environment Defining Population* constructed from PRIMUS and SDSS.

Thresholds for the environment are imposed to classify the target galaxies as high, mid, or low environments. For the quiescent and star-forming target galaxies we calculate the stellar mass functions in different environments and redshift. Afterwards, we compute the QFs using the SMFs for the different environment and redshift ranges. Comparing the QFs in these environment and redshift bins, we find the QF increases over cosmic time (decrease in redshift); however, the change of the QFs for the different environments are independent of the environment of galaxies.

1. INTRODUCTION

Galaxies, in their detailed properties, carry the imprints of their surroundings, with a strong dependence of the quiescent fraction of galaxies on their local environment (e.g. Hubble 1936; Oemler 1974; Dressler 1980; Hermit et al. 1996; Guzzo et al. 1997; for a recent review see Blanton & Moustakas 2009). The strength of this dependence is itself a strongly decreasing function of galaxy stellar mass; at the extreme, the lowest masses ($< 10^9$ $M_\odot$) galaxies are quenched only in dense regions, and never in isolation (Geha et al. 2012). These effects vary with redshift at least in the densest clusters, as observed in the changing fraction of late-type spirals relative to the field found in studies of the morphology-density relation (Dressler 1984; Desai et al. 2007). Clearly understanding the properties of galaxies in the present-day universe requires a careful investigation of the role of environment, and how that role changes over time.

Nevertheless, the evolution of the role of environment is a relatively subtle effect and difficult to study. Although history of galaxies prior to $z \sim 1$ appears to have been one of rapid assembly, since that time the galaxy population has continued to evolve, but less dramatically. Although there are detectable changes in the population, the major classes of galaxies existed at $z \sim 1$, in roughly the same relative numbers as today (Bundy et al. 2006; Borch et al. 2006; Taylor et al. 2009; Moustakas et al. 2013a. Furthermore, at those redshifts we can also detect the dependence of galaxy properties on environment, with lower star-formation rate early-type galaxies populating the denser regions (Cooper et al. 2008; Patel et al. 2009; Kovač et al. 2010).

The most dramatic change in galaxy properties during the past eight billion years has been a remarkable decline in the star-formation rate of galaxies in the Universe (Hopkins & Beacom 2006). This decline appears dominated by decreases in the rates of star-formation of individual galaxies (Noeske et al. (2007)). There is evidence that a large fraction of the decline associated with strongly infrared-emitting starbursts (Bell et al. 2005; Magnelli et al. 2009). The decline does not appear to be due to the quenching of a large fractions of the star-forming population, as reflected in observations of the stellar mass function of quiescent and star-forming galaxies (Blanton et al. (2006),Bundy et al. 2006; Borch et al. 2006; Moustakas et al. 2013a). These findings leave little room for the participation of environmentally-driven quenching in the global census of star-formation. As Cooper et al. (2008) and others have pointed out, because the environmental dependence of total star-formation rates at fixed redshift is relatively small, environmentally effects are unlikely to cause the overall star-formation rate decline.

Thus, the impact of environment on galaxy formation has to be interpreted on top of the background of this overall decline affecting galaxies in all environments. The most straightforward investigation of would directly determine the star-forming properties of galaxies as a function of environment, stellar mass and redshift in a single, consistently analyzed data set. This analysis can reveal how galaxies are quenched in the universe over time, quantitatively establish the contribution of environmental effects to the overall trends, and reveal whether those trends happen equally in all environments. However, such an analysis has not been done previously due to the lack of sufficiently large samples. In this paper, we apply this approach using the Prism Multi-object Survey (PRIMUS; Coil et al. (2011), Cool et al. (2013)), the largest available redshift survey covering the epochs between $0 < z < 1$.

2. SAMPLE SELECTION

In this paper we are interested in measuring the quiescent fraction over a wide range of redshifts and for galaxies in different environments. To do so, we use galaxies

TABLE 1
Summary of Galaxy Subsample

Survey	Redshift (z)	Density	Quiescent N_g	Star-forming N_g
SDSS	$0.0375 - 0.145$	High	5470	4501
		Mid	3614	4438
		Low	5419	8927
PRIMUS	$0.2 - 0.4$	High	322	583
		Mid	177	403
		Low	768	2516
PRIMUS	$0.4 - 0.6$	High	350	675
		Mid	195	405
		Low	871	2385
PRIMUS	$0.6 - 0.8$	High	347	430
		Mid	186	327
		Low	833	1847
PRIMUS	$0.8 - 1.0$	High	136	232
		Mid	94	163
		Low	373	810

at intermediate redshifts from PRIMUS and galaxies at low redshift from SDSS.

We begin with a brief summary of the PRIMUS data in Section 2.1 followed by a summary of the SDSS data in Section 2.2. Then in Section 2.3 we use this data to define the stellar mass complete target galaxy population. Afterwards, in Section 2.4, we classify these target galaxies as quiescent or active star-forming galaxies. Then for each of the classified target galaxies, in Section 2.5, we obtain the environment using a volume-limited *Environment Defining Population*. Finally in Section 2.6, we correct the target galaxy environment for the survey edge effects.

2.1. *PRIMUS*

For galaxies at intermediate redshifts we use multi-wavelength imaging and spectroscopic redshifts data of PRIMUS, which is a faint galaxy survey with precise spectroscopic redshifts ($\sigma_z/(1+z) \approx 0.5\%$) for $\sim 120,000$ galaxies within redshifts $z \approx 0 - 1.2$. The survey was conducted using a IMACS spectrograph on a Magellan I Baade 6.5 m telescope with a slitmask and low dispersion prism. For further details on the PRIMUS observation methods, including survey design, targeting, and data summary, we refer readers to the survey papers: Coil et al. (2011) and Cool et al. (2013).

As done in Moustakas et al. (2013b), we only use fields targeted by PRIMUS with *GALEX* and *Spitzer*/IRAC imaging. This restricts us to five fields. Four of these fields are a part of the *Spitzer* Wide-area Infrared Extragalactic Survey (SWIRE[1]): the European Large Area ISO Survey - South 1 field (ELAIS-S1[2]), the Chandra Deep Field South SWIRE field (CDFS), and the XMM Large Scale Structure Survey field (XMM-LSS). The XMM-LSS consists of two separate but spatially adjacent fields: the Subaru/XMM-Newton DEEP Survey fied (XMM-SXDSS[3]) and the Canadian-France-Hawaii Telescope Legacy Survey field (XMM-CFHTLS[4]). In addition to the SWIRE fields we also include the COSMOS[5] field for a total of five fields.

In all of the PRIMUS target fields we have near-UV (NUV) and far-UV (FUV) measurements from the *GALEX* Deep Imaging Survey (DIS; Martin et al. (2005); Morrissey et al. (2005)). To minimize contamination from neighboring sources, we use a Bayesian photometric code EM$_{\rm PHOT}$ (based on expectation maximization algorithm of Guillaume et al. (2006)). Furthermore, we use ground-based optical and *Spitzer*/IRAC mid-infrared photometric catalogs in each of the fields to obtain integrated fluxes in all photometric bands. To summarize, the general strategy employed is to use a circular aperture photometry to constrain the shape of the SED and then fixing the overall normalization to a estimate of the total magnitude in the detection band. Moustakas et al. (2013b) provides a detailed description of the calculation for each of our target fields.

From the spectroscopic redshift and photometry described above, we use `iSEDfit` to determine stellar masses, star formation rates (SFRs) and other physical properties in a simplified Bayesian framework. `iSEDfit`, which we will only briefly mention in this paper is discussed in detail in Appendix A of Moustakas et al. (2013b). The code uses the redshift and the observed photometry of the galaxies to determine the statistical likelihood of a large ensemble of generated model SEDs. These generated model SEDs depend on population synthesis models and prior parameters. In order to derive our fiducial stellar masses and star formation rates, we use the Flexible Stellar Population Synthesis

[1] http://swire.ipac.caltech.edu/swire/swire.html
[2] http://dipastro.pd.astro.it/esis
[3] http://www.naoj.org/cience/SubaruProject/SDS
[4] http://www.cfht.hawaii.edu/Science/CFHLS
[5] http://cosmos.astro.caltech.edu

(FSPS) models (Conroy & Gunn (2010)) based on the Chabrier (2003) IMF. Other prior parameters are listed in Section 4.1 of Moustakas et al. (2013b). The photometric bands we use for the fitting in our PRIMUS data are the *GALEX* FUV and NUV, the two shortest IRAC bands at 3.6 and 4.5μm, and the five optical bands (in the COSMOS field, we fit seven optical bands and near-infrared bands, see Section 2.3 of Moustakas et al. (2013b)). For a more detailed description of the data used in this paper, we refer readers to Moustakas et al. (2013b) Section 2 and Section 4.1.

2.2. *SDSS-GALEX*

For galaxies at low redshifts we use the SDSS Data Release 7 (DR7; Abazajian et al. (2009)). From the SDSS DR7 data, which provides high fidelity *ugriz* photometry and spectroscopic redshift, we specifically use galaxies from the New York University Value-Added Galaxy Catalog that satisfy the main sample criterion and have galaxy extinction corrected Petrosian magnitudes $14.5 < r < 17.6$ and spectroscopic redshits $0.01 < z < 0.2$ (Blanton et al. (2005b)). Within this sample, we select galaxies with medium depth observations from GALEX. This is done by first retrieving the positions of all *GALEX* tiles from GALEX Release 6 with total exposure time greater than 1 ks and then constructing a joint angular selection function of the SDSS-*GALEX* Sample. This results in a final sample of 167,727 SDSS galaxies with *GALEX* imaging.

For this final sample, we use the MAST/CasJobs[6] interface and a 4″ diamater search radius to obtain the NUV and FUV photometry. For the optical photometry we use *ugriz* bands (from the SDSS `model` magnitudes) scaled to the *r*-band `cmodel` magnitude. We supplement the above UV and optical photometry with integrated JHK_s magnitudes from the 2MASS Extended Source Catalog (XSC; Jarrett et al. (2000)) and with photometry at 3.4 and 4.6μm from the WISE All-Sky Data Release[7]. Further details on the photometry of the SDSS data used in this paper is provided in Moustakas et al. (2013b) Section 2.4.

To obtain the stellar masses and SFRs for the SDSS data, we use `iSEDfit` as done in Section 2.1. Except we use twelve photometric bands: *GALEX* FUV and NUV, SDSS *ugriz*, 2MASS JHK_s, and WISE 3.4 and 4.6μm.

2.3. *Galaxy Samples*

In this seciton we will define the galaxy sample we use for our SMFs and QFs. The population at intermediate redshift is derived from the PRIMUS data and the population at low redshift is derived from the SDSS data, both described above. For the intermediate redshift target galaxy population, we begin with the selection criteria imposed in Moustakas et al. (2013b) for its parent sample. We take the statistically complete *primary* sample from the PRIMUS data, Coil et al. (2011), and then we impose magnitude limits on optical selection bands as specified in Moustakas et al. (2013b) Table 1. These limits are in different optical selection bands and have different values for our five PRIMUS target fields. Next, we join the PRIMUS, *GALEX*, and IRAC window functions to construct the angular selection function. We then exclude stars and broad-line AGN to only select objects spectroscopically classified as galaxies, with high-quality spectroscopic redshifts ($Q \geq 3$) within the redshift range $0.2 - 1.0$. Afterwards we assign statistical weights (described in Coil et al. (2011) and Cool et al. (2013)) to the objects in order to correct for targeting incompleteness and redshift failures. The statistical weight, w_i, for each galaxy is given by

$$w_i = (f_{\rm target} \times f_{\rm collision} \times f_{\rm success})^{-1}, \quad (1)$$

Equation 1 in Moustakas et al. (2013b). In addition to the selection criteria above, we impose stellar mass limits to have a stellar mass complete sample. Stellar mass completeness limits for a magnitude-limited survey such as PRIMUS is a function of redshift, apparent magnitude limit of the survey, and the typical stellar mass-to-light ratio of galaxies near the flux limit.

As done in Moustakas et al. (2013b), we follow Pozzetti et al. (2010) to empirically determine the stellar mass completeness limits. Briefly, for each of the target galaxies we compute $\mathcal{M}_{\rm lim}$ using $log\mathcal{M}_{\rm lim} = log\mathcal{M} + 0.4(m - m_{\rm lim})$. $\mathcal{M}$ is the stellar mass of the galaxy in units of $\mathcal{M}_\odot$, $\mathcal{M}_{\rm lim}$ is the stellar mass of each galaxy if its magnitude was equal to the survey magnitude limit, m is observed apparent magnitude in the selection band, and $m_{\rm lim}$ is the magnitude limit for our five fields mentioned above. We construct a cumulative distribution of $\mathcal{M}_{\rm lim}$ for the 15% faintested galaxies in $\Delta z = 0.04$ redshift bins. In each of these redshift bins, we calculate the minimum stellar mass that includes 95% of the galaxies. Separately for quiescent and star-forming galaxies, we fit quadratic polynomials to the minimum stellar masses versus redshift (classificiation scheme for quiescent and star-forming galaxies is included in the following section). Finally, we use these polynomials to obtain the minimum stellar masses at the center of the redshift bins, $0.2-0.4$, $0.4-0.6$, $0.6-0.8$, and $0.8-1.0$. Note that these redshift bins will later be used to divide the target population during SMF and QF calculations.

For our target galaxy population at low redshift we use our SDSS-*GALEX* data. We limit our target population within the redshift range $0.06 - 0.145$ due to redshift limits later imposed for the volume-limited Environment Defining Population (2.5). The NYU-VAGC provides statistical weight estimates for targeting completeness. In order to have a stellar mass complete low redshift target population, we use a uniform stellar mass limit of $10^9\mathcal{M}_\odot$, which is above the surface brightness and stellar mass-to-light ratio completness limits (Blanton et al. (2005a); Baldry et al. (2008)). The absolute magnitude (M_g) versus redshift for the target galaxy population at both low redshift and intermediate redshift is plotted in Figure 2.1. We again refer readers to Moustakas et al. (2013b) for details; more specifically, Figure 2., Sections 3.1, and 4.3.

2.4. *Classifying Quiescent and Star-Forming Galaxies*

We classify the galaxies from the target sample, defined in the last section, using an evolving cut based on specific star-formation rate utilized in Moustakas et al. (2013b). For a detailed description of the classification scheme, we refer readers to Section 3.2 in Moustakas et al. (2013b).

[6] http://galex.stsci.edu/casjobs
[7] http://wise2.ipac.caltech.edu/docs/release/allsky

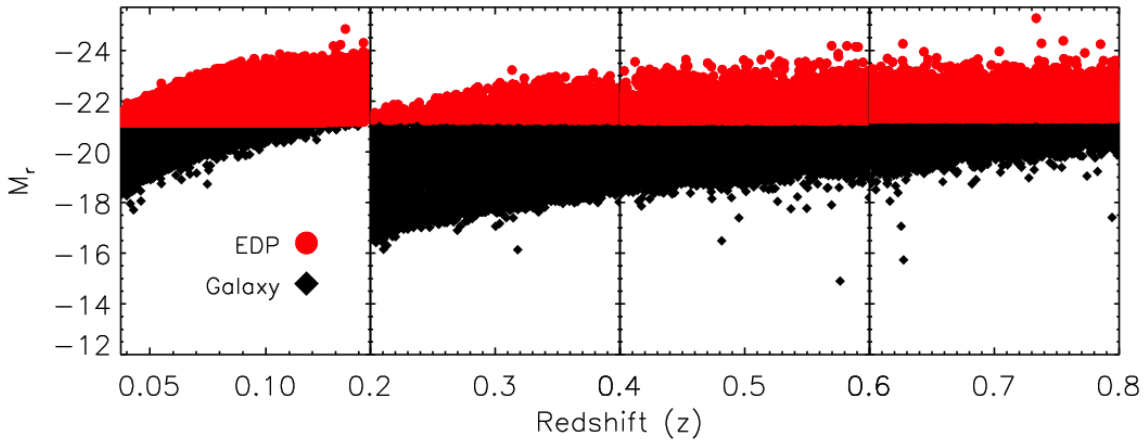

FIG. 1.— Absolute magnitude M_r vs. redshift for the target galaxy population (black) with the Environment Defining Population (red) plotted on top. Both samples are divided into redshift bins:$0.06-0.145$, $0.2-0.4$, $0.4-0.6$, and $0.6-0.8$. The target galaxy population is stellar mass complete (Section 2.3 while the EDP is volume limited through M_g limits (Section 2.5).

To summarize, this classification method utilizes the star-forming (SF) sequence, which is the correlation between star-formation rate (SFR) and stellar mass in star-forming galaxies observed at least until $z \sim 2$. As stated in Moustakas et al. (2013b), the PRIMUS sample displays a well-defined SF sequence within the redshift range of our target population. Using the power-law slope for the SF sequence derived by Salim et al. (2007) (SFR $\propto \mathcal{M}^{0.65}$) and the minimum of the quiescent/star-forming bimodality, determined by eye, we obtain the following equation to classify the target galaxies (Equation 2 in Moustakas et al. (2013b)):

$$\log(\mathrm{SFR}_{\mathrm{min}}) = -0.49 + 0.64\log(\mathcal{M} - 10) + 1.07(\mathrm{z} - 0.1), \quad (2)$$

where $\mathcal{M}$ is the stellar mass of the galaxy. If the target galaxy SFR and stellar mass place the galaxy above Equation 2 we classify it as star-forming; if below, as quiescent (Moustakas et al. (2013b) Figure 1.).

2.5. *Galaxy Environment*

We define the environment of a galaxy as the number of neighboring galaxies contained within a fixed aperture centered around it. We use fixed cylindrical apertures with dimensions specified in Table 2 to probe the environment of the target sample galaxies. A fixed cylindrical apertures was chosen over a spherical one, often used in literature (e.g. Croton et al. (2005)), due to redshift errors in the PRIMUS data and considerations of redshift space distortions within our PRIMUS data redshift range, $[0.2, 1.0]$. Furthermore, we use aperture dimensions listed in Table 2 based on the analysis of scale dependence for clustering in Blanton et al. (2006). As Blanton et al. (2006) suggests, galactic properties such as their star-formation histories are dependent on properties such as the masses of their host dark matter halos. Hence, by employing fixed cylindrical apertures with $r_{\mathrm{ap}} = 1, 2$Mpc we are able to probe the local small scale environment within the scales of the host dark matter halos. As a comparison, we also include fixed cylindrical apertures with $r_{\mathrm{ap}} \geq 5$Mpc to probe large scale environment, which Blanton et al. (2006) finds to be unrelated to the recent star formation history of galaxies.

In order to obtain the fixed aperture based environment for the galaxies in the target population, we first establish a volume limited *Environment Defining Population* (EDP) by imposing a fixed cumulative number density absolute magnitude cut off. By using a fixed cumulative number density for this sample we seek to build an EDP with galaxies that have similar populations in all of the redshift bins i.e. accounting for the progenitor bias. As Behroozi et al. (2013) and Leja et al. (2013) find in their analysis of the cumulative number density method using a dark matter simulation with abundance matching and a semi-analytic model, respectively, cumulative number density method, while it does not precisely account for the scatter in mass accretion or galaxy-galaxy mergers, provides a promising tool to compare galaxy populations over a wide range of cosmic time. In addition we use the highest redshift bin cumulative number density as the fixed number density Furthermore Behroozi et al. (2013)

The EDP for the PRIMUS sample is derived from the same parent sample as the target galaxies. We restrict the PRIMUS EDP galaxies within the redshift range $0.2 - 1.0$ and divide them into redshift bins of width $\Delta z = 0.2$. For each of these redshift bins, we impose separate absolute magnitude ($M_{g,\mathrm{lim}}$) limits such that the cumulative number density of the sample ordered by M_g is equal to the cumulative number density of the highest redshift bin with an empirically determined limit. First, to determine the highest redshift bin $(0.8 - 1.0)$ limit we look at the M_g distribution with bin size $\Delta M_g = 0.25$ and select $M_{g,\mathrm{lim}}$ to be the M_g value near the peak of the distribution where number density of the bins with fainter objects (greater M_g value) are smaller than the number density of the bin at $M_{g,\mathrm{lim}}$. We find this $M_{g,\mathrm{lim}}(0.8 < z < 1.0)$ to be, conservatively, $M_g = -20.75$. With this value we then calculate the rest of the $M_{g,\mathrm{lim}}$s by finding the M_g value where the cumulative number density ordered by absolute magnitude of the redshift bins equals that of the the highest redshift bin at $M_{g,\mathrm{lim}}(0.8 < z < 1.0)$. Note that when calculating

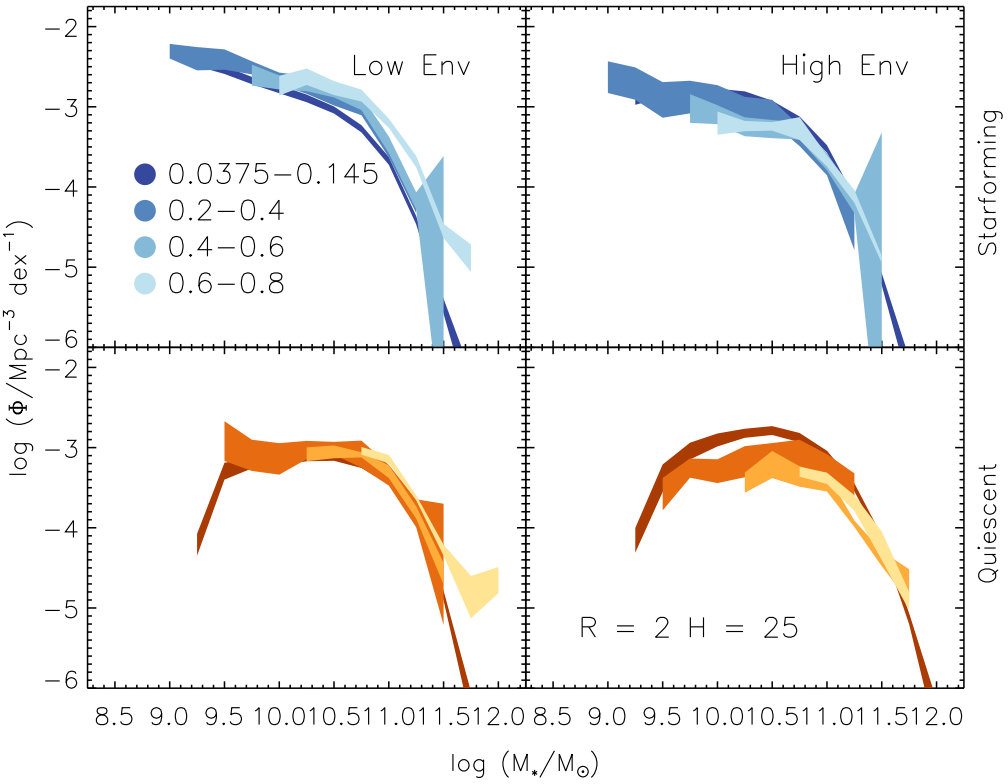

FIG. 2.— Evolution of stellar mass functions of star-forming (top) and quiescent (bottom) target galaxies in low (left) and high (right) environments from redshift range $z = 0-0.8$. The environment of each galaxy was calculated using a cylindrical aperture size of $R = 2$Mpc and $H = 25$Mpc and classification based on the cut-offs specified in Table 2. The SMFs use mass bins of width $\Delta\log(\mathcal{M}/\mathcal{M}_\odot) = 0.25$. In each panel we use shades of blue (star-forming) and orange (quiescent) to represent the SMF at different redshift, higher redshifts being progressively lighter.

the number densities, the number of galaxies takes into account the statistical weights (described in Section 2.1 and 2.2).

For the EDP of the SDSS-*GALEX* sample (hereafter simply referred to as the SDSS EDP), we do not use the parent sample of the data due to the geometry of the combined angular selection function of the SDSS VAGC and *GALEX*. Instead, since we are not interested in the FUV, NUV values for the EDP, we just use the SDSS VAGC where the SDSS-*GALEX* catalog is derived from. Furthermore, we impose a redshift limit $0.0375-0.145$ on the SDSS EDP sample as opposed to the redshift range of $0.01 - 0.2$ in Moustakas et al. (2013b). This is due to the lack of faint galaxies at $z \sim 0.2$ and the lack of bright galaxies at $z \sim 0.01$. In other words, the lower bound for the redshif range was empirically determined by the bright limit of the M_g versus redshift distribution and the upper bound by the faint limit of the M_g versus redshift distribution. The same fixed cumulative number density method is used on this SDSS EDP. Ultimately we use $M_{g,\rm lim} = -20.57$, -20.73, -20.80 and -20.95 for the redshift bins $0.06 - 0.145$, $0.2 - 0.4$, $0.4 - 0.6$, $0.6 - 0.8$, respectively. These absolute magnitude limits are illustrated in Figure 2.1, which plots the absolute magnitude versus the redshift for the EDP galaxies and the target galaxies.

Using the above definition of environment and the EDP galaxies, we obtain the environment for each of the target population galaxies by counting the number of EDP galaxies, n_{env}, within the fixed cylinder aperture surrounding it. Since we use apertures of different dimensions, we are interested in the relative densitites rather than the actual n_{env} values. Hence, we use the percentage rank of the galaxy environment to quantify overdense environments and underdense environments. More specifically, for each of the redshift bins ($0.2 - 0.4$, $0.4 - 0.6$, $0.6 - 0.8$, and $0.8 - 1.0$) the n_{env} values for all target galaxies in that bin are listed and assigned a percentage rank based on their position in the list: $n_{env} = 0$ corresponding to 0% and the maximum n_{env} for a target galaxy in the z-bin corresponding to 100%. Using these percentage ranks, each target galaxy is classified as high-, mid-, or low-environment based on the cut-offs specified in Table 2. Target sample galaxies are classified as high-environment if its percentage rank lies within the top 20% and as low-environment if its percentage rank lies within the bottom 20%. In Table 2, apertures with radius $1h^{-1}$Mpc have a low-eneivonrment cut-off of higher than 20%. This is because over 20% of target sample galaxies have $n_{env} = 0$ such a smaller aperture size. Hence we defined the low-environment percentage rank cut-off to contain all galaxies with $n_{env} = 0$. In order to have a fair comparison for the different z-bins when using this aperture, the low-environment cut-off was selected as the lowest cut-off that includes all galaxies with $n_{env} = 0$ for all z-bin. More specific details for the high- and low-

environment cut-offs are provided in Table 2.

Similar fixed aperture methods have also been used in Croton et al. (2005) for galaxies in the 2dF Galaxy Redshift Survey (Colless et al. (2003)) and in Muldrew et al. (2012) for a mock galaxy catalogue generated from embedding galaxies onto the Millenium Dark Matter Simulation (Springel et al. (2005)).

2.6. *Edge Effects*

One of the challenges in obtaining the galaxy environment using a fixed aperture method is accounting for the edge effects of the survey. For the target galaxies located near the edge of the survey, part of the fixed aperture encompassing it will lie outside the survey regions. In this case, the n_{env} will only reflect the galaxies which lie in the fraction of the aperture contained within the survey geometry.

In order to account for these edge effects, we use a Monte Carlo method to impose edge cuts on the target galaxy population. We first divide the target sample galaxies into n_{bin} redshift bins, specified in Table 2. For each of the bins we compute the angular separation, $\theta_{\rm ap}$ that corresponds to the radius of the aperture at the central redshift of the bin. Then the target galaxies in each bin are matched up to a sample of $N_{ransack} = 1,000,000$ points with arbitrary RA and Dec values within the target sample fields, hereafter referred to as the ransack sample (named based on the procedure used to construct them). We count the number of ransack points, $n_{\rm ransack}$, within $\theta_{\rm ap}$ for the target galaxies in each of the redshift bins. $n_{\rm ransack}$ values for the target galaxies are then compared to the expected value:

$$E[n_{\rm ransack}] = \frac{N_{\rm ransack}}{A_{\rm fields}} \times \pi\theta_{\rm ap}^2 \times f_{\rm thresh} \qquad (3)$$

where $A_{\rm fields}$ is the total angular area of the target fields and $f_{\rm thresh}$ is the fractional threshold for the edge effect cut-off, specified in Table 2. If $n_{\rm ransack}$ for a target galaxy is greater than $E[n_{\rm ransack}]$ then the target galaxy remains in the sample; otherwise, it is discarded.

3. RESULTS

In this section, we describe our calculation to obtain the stellar mass functions (SMF) and quiescent fraction (QF) using the stellar mass complete target population. In Section .1 we construct the non-parametric estimate of SMFs for star-forming and quiescent galaxies in redshift bins: $0.06 - 0.145$, $0.2 - 0.4$, $0.4 - 0.6$, $0.6 - 0.8$, and $0.8 - 1.0$. Form these SMFs, we calculate the QFs in section 3.2.

3.1. *Stellar Mass Function*

Our primary interest in the SMFs is to investigate the evolution of the quiescent fraction in different density environments over our redshift range. Hence, we first divide the target galaxy sample into quiescent and star-forming target samples using the classification scheme from Section 2.4. Both the quiescent and star-forming target samples are then divided into "high-environment","mid-environment", and "low-environment" based on their environment classification described in Section 2.5. We use the five redshift bins described in **??** to get a total of 30 subsamples that are classified based on star-forming/quiescent, environment, and redshift. For each of these subsamples, we calculate the SMFs and their errors.

To calculate the SMFs we employ a non-parametric $1/V_{\rm max}$ estimator commonly used for galaxy luminosity functions, as done in Moustakas et al. (2013b) and discussed in the review Johnston (2011). The differential SMF is given by the following equation:

$$\Phi(\log \mathcal{M})\Delta(\log \mathcal{M}) = \sum_{\rm i=1}^{\rm N} \frac{\rm w_i}{\rm V_{max,avail,i}}. \qquad (4)$$

The equation above is the same as Equation 3. in Moustakas et al. (2013b) other than the use of $V_{\rm max,avail}$ instead than $V_{\rm max}$, which is used because of edge effect considerations along the edges of the survey. w_i represnts the statistical weight of each galaxy i and $\Phi(\log\mathcal{M})\Delta(\log\mathcal{M})$ is the number of galaxies (N) per unit volume within the stellar mass range $[\log \mathcal{M}, \log \mathcal{M} + \Delta(\log \mathcal{M})]$.

$V_{\rm max,i}$ is the maximum cosmological volume where it is possible to observe each galaxy i given the apparent magnitude limits of the survey. However in Section 2.6 we remove the galaxies that lie on the edge of from the target sample. In doing so we reduce the maximum cosmological volume where a galaxy can be observed, thereby reducing $V_{\rm max,i}$ to a what we will refer to as $V_{\rm max,avail,i}$.

To calculate $V_{\rm max,avail,i}$, we generate a sample of points with random RA, Dec, and z (not to be confused with the ransack sample in Section 2.6) within the target fields and the redshift limits of the surveys. We then impose the same edge effect cut-off used on the target galaxy population, described in Section 2.6, onto this random sample. For each redshift bin j out of the $n_{\rm bin}$ redshift bins, we compute the fraction of the random points that remain in the bin after the points near the edges are removed: $f_{\rm edge,j}$. Finally we calculate: $V_{\rm max,avail,i} = V_{\rm max,i} \times f_{\rm edge,j}$. The $V_{\rm max,i}$ values in the equation above are computed following the method described in Moustakas et al. (2013b) with the same redshift-dependent K-correction from observed SED and luminosity evolution model. For more details on computing $V_{\rm max}$ we refer readers to Section 4.2 in Moustakas et al. (2013b).

In order to calculate the uncertainty of the SMFs from the sample variance, we use a standard jackknife technique as done in Moustakas et al. (2013b). For the PRIMUS target galaxies, we calculate SMFs after excluding one of the target fields each time. Note in these SMF calculations, the $1/V_{\rm max,avail}$ is corrected for the fact that excluding a field changes the total area of the survey. Then using the calculated SMFs we calculate the uncertainty:

$$\sigma^j = \sqrt{\frac{M-1}{M}\sum_{k=1}^{M}(\Phi_k^j - \langle\Phi^j\rangle)^2} \qquad (5)$$

M in this equation is the number of jack knife SMFs in the mass bin; this value is different for each of the stellar mass bins since not all mass bins have galaxies from all five target fields. $\langle\Phi^j\rangle$ is the mean number density of galaxies in each stellar mass bin for all of the jack knife Φ^js.

Since the SDSS-*GALEX* data are contained in one field, we first divide the field into a 30×20 rectangu-

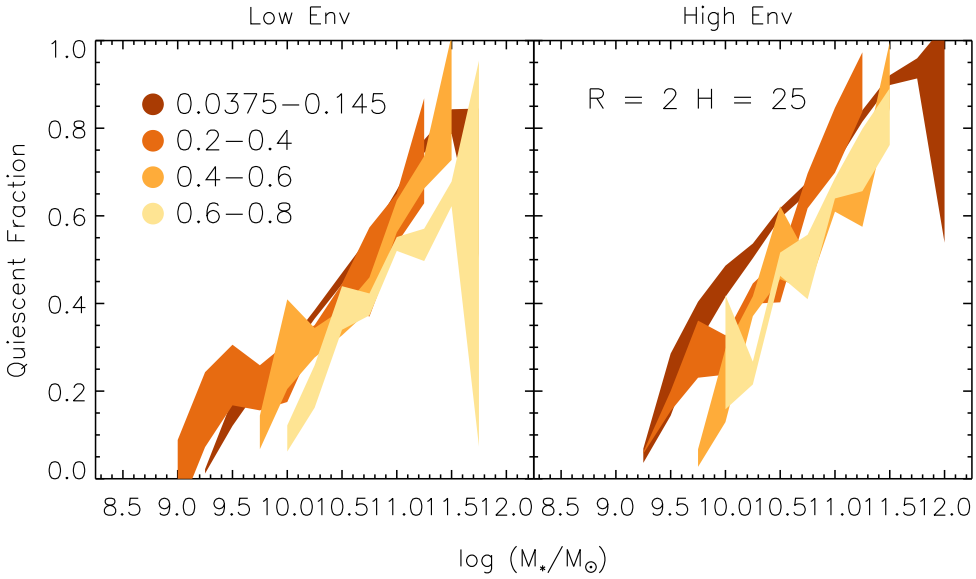

FIG. 3.— Evolution of the quiescent fraction for target galaxies in low (left) and (high) environments from redshift range $z = 0 - 0.8$. The QFs were calculated using the SMFs specificed in Figure .1. We use lighter shades of orange for the QFs at higher redshifts.

lar grid and then only keep the sectors with at least 100 galaxies in them. Then we use the same method as above to compute the uncertainties through the jack knife technique. The panels in the top two rows of Figure .1 show the SMFs with uncertainties for all 30 subsamples using aperture with dimensions $R_{\rm ap} = 1$Mpc and $h_{\rm ap} = 50$Mpc.

3.2. *Quiescent Fraction*

In the last section, we calculated the SMFs for all subsamples of the target galaxies classified by star-forming/quiescent, environment, and redshift. In this section, we use the Φ calculated for each subsample above to compute their respective QFs:

$$\mathrm{QF} = \frac{\Phi_{\rm Q}}{\Phi_{\rm SF} + \Phi_{\rm Q}}. \quad (6)$$

Φ_Q and Φ_{SF} are the total number of galaxies per unit volume in stellar mass bin $\Delta(\log \mathcal{M})$ (Equation 4) for the quiescent and star-forming subsamples, respectively. A value for the QF is not assigned in stellar mass bins where either the star-formation subsample or the quiescent subsample do not have any galaxies. The bottom panels of Figure .1 shows the QFs for the different redshift bins and environment density classifications.

In order to compare the QFs at different redshift for each of the environment classifications, we perform a linear least squares fit on the QF for all the QFs. Then we use the value of the linear fit at an empirically selected fiducial mass $\log \mathcal{M}/\mathcal{M}_\odot = 10.5$ (using fiducial mass of $\log \mathcal{M}/\mathcal{M}_\odot = 11.0$ does not noteably change the outcome). These values are used to highlight and attempt to quantify the differences of the QFs at the different redshifts, Figure .1

The figures and analysis described in this paper are done using galaxy environment determined from a fixed aperture with $r_{\rm ap} = 1$Mpc and $h_{\rm ap} = 50$Mpc. The same analysis was repeated for various aperture dimensions: $r_{\rm ap} = 0.5, 1, 2, 3$Mpc and $h_{\rm ap} = 25, 50$Mpc. Minor adjustments to the environment classification thresholds were adopted in these analyses for the smaller apertures ($r_{\rm ap} = 0.5, 1$Mpc and $r_{\rm ap} = 25$Mpc). The results obtained from using these different are consistent with the results displayed in this paper.

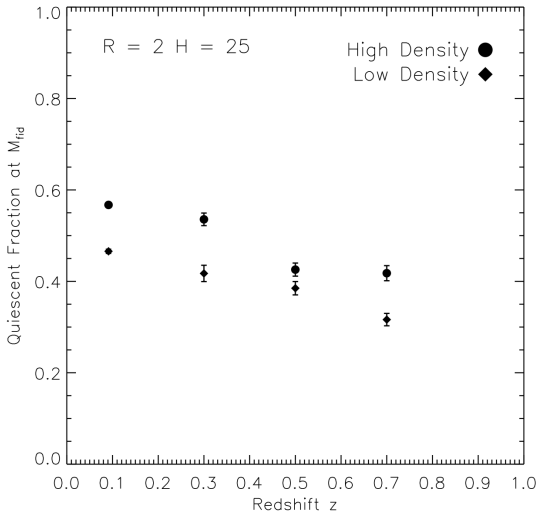

FIG. 4.— Quiescent fraction at fiducial mass $\log(\mathcal{M}/\mathcal{M}_\odot) = 10.5$ for low (square) and high (circle) environments in the redshift range $z = 0 - 0.8$. The evolution of $f_Q(\mathcal{M}_{\rm fid})$ for galaxies in different environments shows an evolution over the redshift range that is independent of environment density. Futhermore throughout the redshift range the difference in $f_Q(\mathcal{M}_{\rm fid})$ remains relatively constant and < 0.15.

4. DISCUSSION AND CONCLUSIONS

We have measured the SMFs and QFs using low redshift SDSS-*GALEX* galaxies and intermeidate redshift PRIMUS galaxies. Specifically we anlayzed the evolution of the QFs over the redshift range $0.0 - 1.0$ for galaxies in environment densities (Figure .1). We find that there is an expected increase in QF with decrease in the red-

TABLE 2
Fixed Cylindrical Aperture Dimensions

Radius (Mpc)	Height (Mpc)	n_{bin}	Edgecut	High Env Threshold (galaxies)	Low Env Threshold (galaxies)
1.0	50	6	80%	1.5	0.0
2.0	50	6	75%	4.0	0.0

shift for subsamples in all environment densities. More importantly we find that the change in QF over redshift is independent of the environment and remains relatively equal for all environments.

- Comparison to other works.

  – Alberts et al. 2013

REFERENCES

Abazajian, K. N., Adelman-McCarthy, J. K., Agüeros, M. A., et al. 2009, ApJS, 182, 543
Baldry, I. K., Glazebrook, K., & Driver, S. P. 2008, MNRAS, 388, 945
Behroozi, P. S., Marchesini, D., Wechsler, R. H., et al. 2013, ApJ, 777, L10
Bell, E. F., Papovich, C., Wolf, C., et al. 2005, ApJ, 625, 23
Blanton, M. R., Eisenstein, D., Hogg, D. W., & Zehavi, I. 2006, ApJ, 645, 977
Blanton, M. R., Lupton, R. H., Schlegel, D. J., et al. 2005a, ApJ, 631, 208
Blanton, M. R., & Moustakas, J. 2009, ARA&A, 47, 159
Blanton, M. R., Schlegel, D. J., Strauss, M. A., et al. 2005b, AJ, 129, 2562
Borch, A., Meisenheimer, K., Bell, E. F., et al. 2006, A&A, 453, 869
Bundy, K., Ellis, R. S., Conselice, C. J., et al. 2006, ApJ, 651, 120
Chabrier, G. 2003, PASP, 115, 763
Coil, A. L., Blanton, M. R., Burles, S. M., et al. 2011, ApJ, 741, 8
Colless, M., Dalton, G., Maddox, S., et al. 2003, VizieR Online Data Catalog, 7226, 0
Conroy, C., & Gunn, J. E. 2010, FSPS: Flexible Stellar Population Synthesis, astrophysics Source Code Library, ascl:1010.043
Cool, R. J., Moustakas, J., Blanton, M. R., et al. 2013, ApJ, 767, 118
Cooper, M. C., Newman, J. A., Weiner, B. J., et al. 2008, MNRAS, 383, 1058
Croton, D. J., Farrar, G. R., Norberg, P., et al. 2005, MNRAS, 356, 1155
Desai, V., Dalcanton, J. J., Aragón-Salamanca, A., et al. 2007, ApJ, 660, 1151
Dressler, A. 1980, ApJ, 236, 351
Dressler, A. 1984, ARA&A, 22, 185
Geha, M., Blanton, M. R., Yan, R., & Tinker, J. L. 2012, ApJ, 757, 85
Guillaume, M., Llebaria, A., Aymeric, D., Arnouts, S., & Milliard, B. 2006, in Society of Photo-Optical Instrumentation Engineers (SPIE) Conference Series, Vol. 6064, Image Processing: Algorithms and Systems, Neural Networks, and Machine Learning, ed. E. R. Dougherty, J. T. Astola, K. O. Egiazarian, N. M. Nasrabadi, & S. A. Rizvi, 332–341
Guzzo, L., Strauss, M. A., Fisher, K. B., Giovanelli, R., & Haynes, M. P. 1997, ApJ, 489, 37
Hermit, S., Santiago, B. X., Lahav, O., et al. 1996, MNRAS, 283, 709
Hopkins, A. M., & Beacom, J. F. 2006, ApJ, 651, 142
Hubble, E. P. 1936, The Realm of the Nebulae (New Haven: Yale University Press)
Jarrett, T. H., Chester, T., Cutri, R., et al. 2000, AJ, 119, 2498
Johnston, R. 2011, A&A Rev., 19, 41
Kovač, K., Lilly, S. J., Knobel, C., et al. 2010, ApJ, 718, 86
Leja, J., van Dokkum, P., & Franx, M. 2013, ApJ, 766, 33
Magnelli, B., Elbaz, D., Chary, R. R., et al. 2009, A&A, 496, 57
Martin, D. C., Fanson, J., Schiminovich, D., et al. 2005, ApJ, 619, L1
Morrissey, P., Schiminovich, D., Barlow, T. A., et al. 2005, ApJ, 619, L7
Moustakas, J., Coil, A. L., Aird, J., et al. 2013a, ApJ, 767, 50
—. 2013b, ApJ, 767, 50
Muldrew, S. I., Croton, D. J., Skibba, R. A., et al. 2012, MNRAS, 419, 2670
Noeske, K. G., Weiner, B. J., Faber, S. M., et al. 2007, ApJ, 660, L43
Oemler, A. 1974, ApJ, 194, 1
Patel, S. G., Holden, B. P., Kelson, D. D., Illingworth, G. D., & Franx, M. 2009, ApJ, 705, L67
Pozzetti, L., Bolzonella, M., Zucca, E., et al. 2010, A&A, 523, A13
Salim, S., Rich, R. M., Charlot, S., et al. 2007, ApJS, 173, 267
Springel, V., White, S. D. M., Jenkins, A., et al. 2005, Nature, 435, 629
Taylor, E. N., Franx, M., van Dokkum, P. G., et al. 2009, ApJ, 694, 1171

APPENDIX

Stellar Mass Function

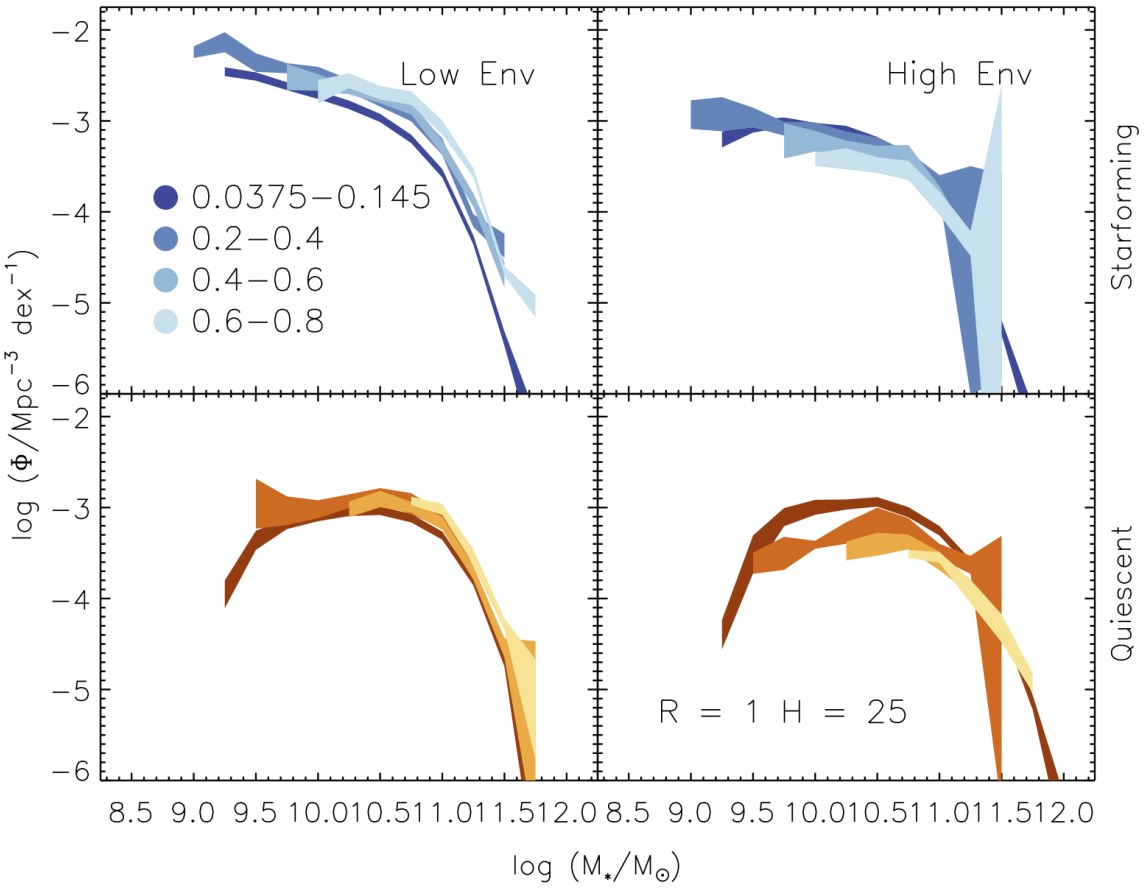

FIG. 5.— SMF for $r_{\rm ap} = 1$Mpc and $h_{\rm ap} = 25$Mpc

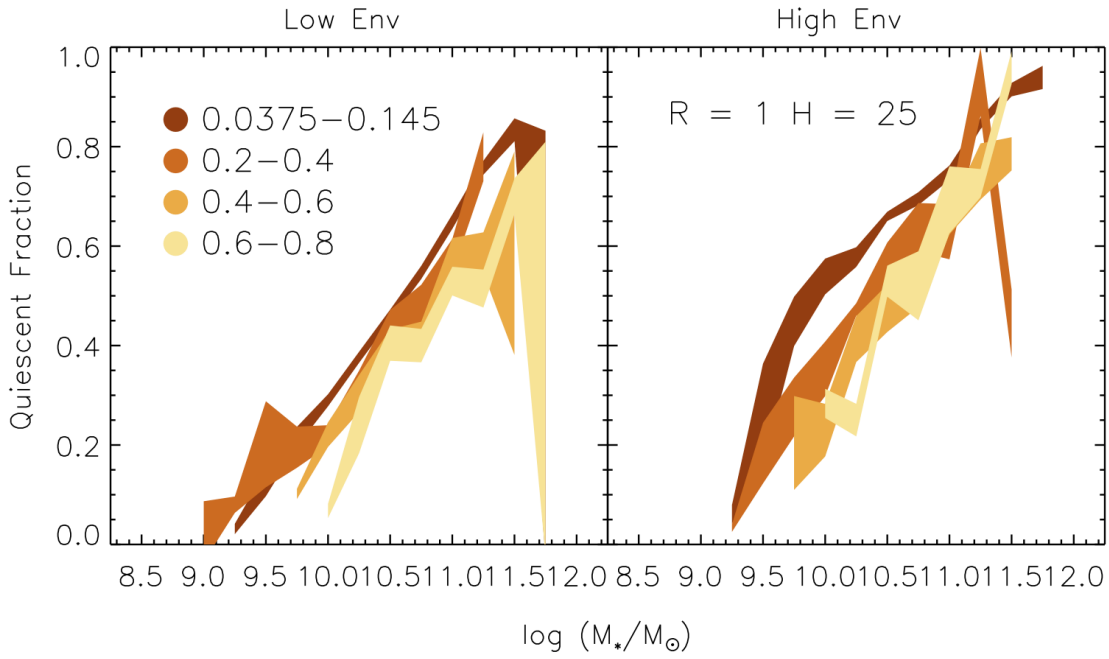

FIG. 6.— QF for $r_{\rm ap} = 1$Mpc and $h_{\rm ap} = 25$Mpc

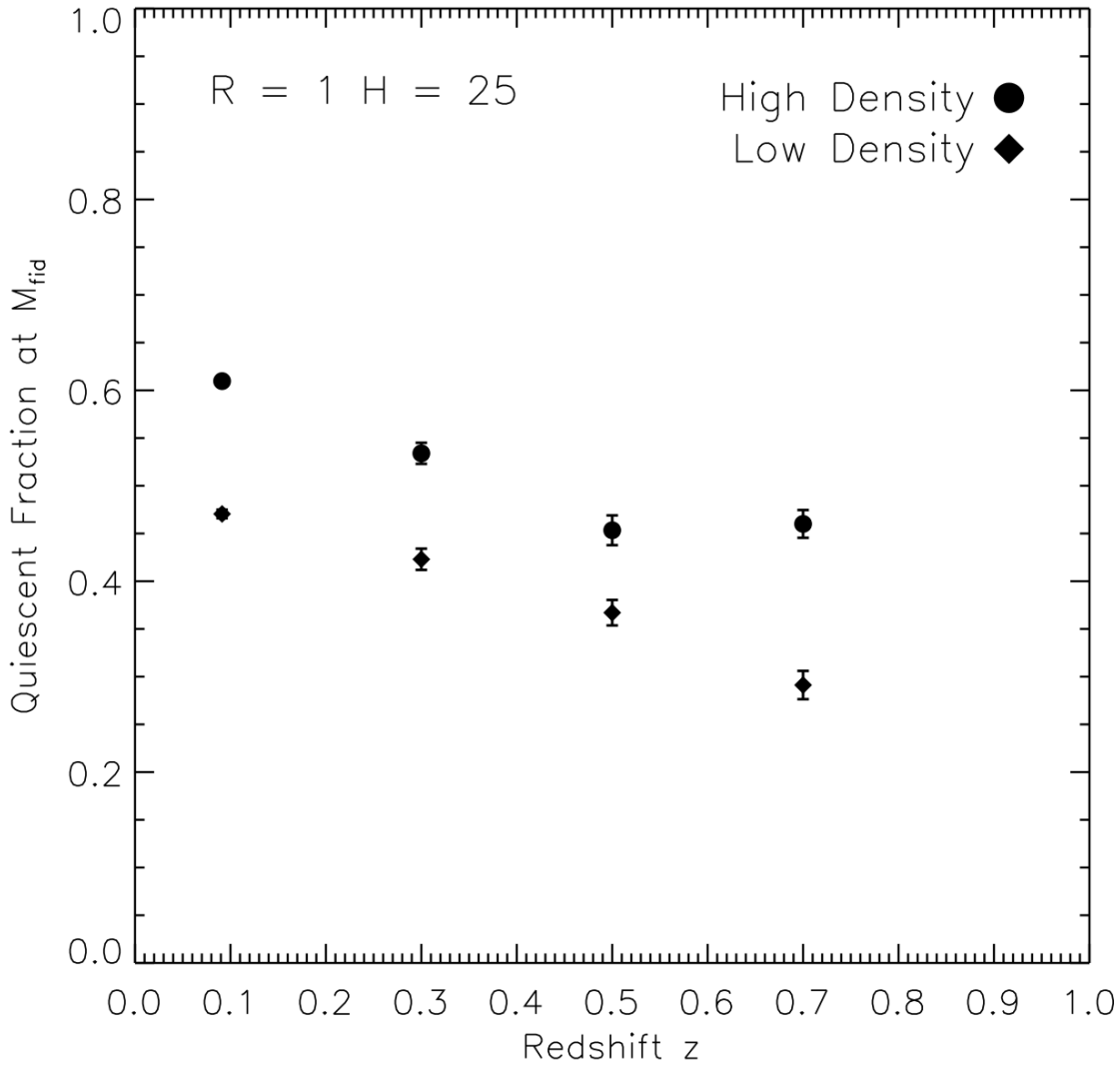

FIG. 7.— QF at fiducial mass for $r_{\rm ap} = 2$Mpc and $h_{\rm ap} = 50$Mpc